

Article

Microstructure Refinement by a Combination of Heat Treatment and Thixoforming Process Followed by Severe Plastic Deformation and Their Effects on Al-Si Alloy Hardness

Mohamed Abdelgawad Gebрил ^{1,*}, Mohd Zaidi Omar ² , Intan Fadhlin Mohamed ², Norinsan Kamil Othman ³ 
and Osama M. Irfan ^{4,5,*}

¹ Department of Mechanical Engineering, Faculty of Engineering, Benghazi University, Benghazi 16063, Libya

² Department of Mechanical and Manufacturing Engineering, Faculty of Engineering and Built Environment, Universiti Kebangsaan Malaysia, Bangi 43600, Selangor, Malaysia

³ Department of applied physics, Faculty of Science and Technology, Universiti Kebangsaan Malaysia, Bangi 43600, Selangor, Malaysia

⁴ Department of Mechanical Engineering, College of Engineering, Qassim University, Buraydah 51452, Saudi Arabia

⁵ Mechanical Department, Beni Suef University, Beni Suef 62746, Egypt

* Correspondence: mohamed.almalki@uob.edu.ly (M.A.G.); o.ahmed@qu.edu.sa (O.M.I.); Tel.: +218-9208-51348 (M.A.G.); +966-556-280-516 (O.M.I.)



Citation: Gebрил, M.A.; Omar, M.Z.; Mohamed, I.F.; Othman, N.K.; Irfan, O.M. Microstructure Refinement by a Combination of Heat Treatment and Thixoforming Process Followed by Severe Plastic Deformation and Their Effects on Al-Si Alloy Hardness. *Metals* **2022**, *12*, 1972. <https://doi.org/10.3390/met12111972>

Academic Editor:
Andrey Pozdniakov

Received: 23 September 2022

Accepted: 12 November 2022

Published: 18 November 2022

Publisher's Note: MDPI stays neutral with regard to jurisdictional claims in published maps and institutional affiliations.



Copyright: © 2022 by the authors. Licensee MDPI, Basel, Switzerland. This article is an open access article distributed under the terms and conditions of the Creative Commons Attribution (CC BY) license (<https://creativecommons.org/licenses/by/4.0/>).

Abstract: This study fabricated a thixoformed Al-7% Si alloy using the cooling slope technique and subjected it to heat treatment before processing with severe plastic deformation to determine the effect of this combination method on the microstructure refinement and hardness of Al-Si alloys (300 Series). Each as-cast and thixoformed Al-Si alloy sample was subjected to equal-channel angular pressing (ECAP) and high-pressure torsion (HPT) individually at room temperature before and after heat treatment. ECAP was conducted in a mould with a 120° channel angle via route A, and HPT was applied with 0.75 and 5 turns. The heat-treated thixoformed Al-Si alloy subjected to the HPT process had an ultra-fine grain microstructure and showed a fine and homogeneous redistribution of the eutectic phase in the Al matrix. For the as-cast alloy, the hardness of the heat-treated thixoformed Al-7% Si alloy increased from 63 HV to 124 and 215 Hv after two ECAP passes and five turns of HPT due to the reduced and redistributed eutectic phase in the Al matrix. Subjecting the Al-7% Si alloy to a combination of semisolid and heat treatment processes before subjecting it to severe plastic deformation resulted in microstructural refinement and improved the hardness of the Al-Si alloy. The results indicate that HPT is a more effective method than ECAP for increasing the hardness of the thixoformed Al-Si alloy due to microstructure refinement.

Keywords: Al-Si alloy; thixoforming; heat treatment; ECAP; HPT; hardness

1. Introduction

Al-Si alloys are extensively used to manufacture automotive components through various casting processes. Despite its extensive use, one drawback of using hypoeutectic Al-Si alloys is low fracture toughness and strength because of the presence of primary α -Al in dendritic form surrounded by second-phase eutectic silicon flakes. Coarse-flake Si particles can cause premature crack initiation during deformation and reduce the alloy's fracture toughness, which decreases its workability and ductility at room temperature [1–3]. The morphology and distribution of Si particles are crucial determiners of the mechanical properties of the Al-Si alloy.

The semisolid process is a major technique in the automotive industry for refining the microstructure of Al-Si alloys. In the semisolid processing of Al-Si alloys, the primary α -Al phase transforms from a dendritic to a globular (spherical) shape, and eutectic Si particles are refined into acicular-shaped particles [4]. There are several techniques for creating a

suitable non-dendritic microstructure, and one of them is the cooling slope casting (CS) process. CS is a simple semisolid metal casting process with minimum equipment and operating costs [4–9]. SSM processing enhances the mechanical properties of aluminium alloys [7–9]. Since Al-Si alloys are heat-treatable, applying heat treatment to modify eutectic Si particles and the morphologies of intermetallic compounds increases the strength of the aluminium alloys through a precipitation hardening process [10]. The primary reason for good fracture elongation in the T6 solution heat treatment of cast Al-Si alloys is the spheroidisation of eutectic silicon [11]; the T6 solution heat treatment also improves the tensile strength elongation [12].

The combination of the T6 heat treatment and semisolid processing of Al-Si alloys enhances their mechanical properties due to the change in eutectic Si morphology in A356 and A357 alloys [13,14]. The homogeneity and refinement of the microstructure through deformation enhance the mechanical properties of hypoeutectic Al-Si alloys [15,16]. Plastic deformation methods, such as ECAP and accumulative roll bonding, can refine microstructures [17–19]. The two major processes in SPD are equal-channel angular pressing (ECAP) and high-pressure torsion (HPT). SPD enhances the mechanical properties of the Al-Si alloy by refining the microstructure and homogeneously dispersing the eutectic phase [20–23].

There is a lack of investigations on the outcomes of combining heat treatment with the refining process and severe plastic deformation. Several studies combined semisolid and ECAP processes to improve mechanical properties [21,23,24]. The combination of annealing heat treatment and ECAP enhances the wear resistance and hardness of the A356 alloy [22], while combining annealing with ECAP improves the corrosion resistance of 6061 aluminium alloy [25]. Combining T6 heat treatment with HPT increases the hardness and corrosion resistance of A356 alloy [26]. The present study describes how microstructure refinement methods that use a combination of thixoforming and T6 heat treatment, followed by severe plastic deformation via ECAP and the HPT process, affect the Al-Si alloy and its hardness. This study is significant because it discusses the effect of applying thixoforming and heat treatment to as-cast flaky Si particles before subjecting them to severe plastic deformation.

2. Materials and Methods

The Al-Si alloy used in this study is the as-cast commercial Al-Si alloy (Si-7 wt.%, Mg-0.26 wt.%, Fe-0.243 wt.%, Cu-0.05 wt.%, Mn-0.002 wt.% and Zn-0.002 wt.%). This study used a semisolid process to melt the alloy in a 750 °C graphite crucible under an argon atmosphere to prevent oxidation. The researchers used differential scanning calorimetry (DSC) to determine the pouring temperature of molten metal, solidus and liquidus temperatures and the liquid fraction profile in the semisolid transition range. In the cooling slope casting process, the alloy is heated to a semisolid temperature, and the molten metal is poured on a 250 mm stainless steel slope with a 60° tilt angle into a mould with a vertical surface. The reason for selecting these conditions was based on our team's work [27]. The equipment used for this process is shown in Figure 1a. This study chose a 620 °C pouring temperature for the molten metal to limit overheating [27]. The molten metal was poured down the stainless steel slope into a mould with a 30 mm diameter and 155 cm high vertical surface before quenching it in water. Cylindrical ingots were cut into 120 mm lengths. The samples for thixoforming had a dimension of $\text{Ø } 30 \times 20$ mm. The samples were rapidly heated for five minutes at 585 °C to obtain spheroidised α -Al grains, after which the samples were compressed using a hydraulic cylinder press with a 20 kN load and 85 mm/s maximum compression speed.

The heat treatment of the as-cast and thixoformed samples followed the T6 procedure, where the solution treatment was carried out at 540 °C for eight hours, followed by water quenching, and the samples were aged at a 180 °C temperature for three hours [28]. After the heat treatment, the as-received and thixoformed cast samples were machined to obtain rods with a 10 mm diameter. Some as-cast and heat-treated rod bars were subjected to ECAP at room temperature via route A without rotation between successive passes, as

shown in Figure 1b. The samples were pressed through a circular cross-section die channel with a 120° inner angle. For HPT samples, the 10 mm diameter rods were cut into discs with 1 mm thickness using an electric discharge wire cutting machine (EDM). HPT was carried out under a 6.0 GPa pressure for 0.75 and 5 revolutions at a 1 rpm rotation speed at room temperature to reduce the sample thickness to 0.81–0.85 mm. This study used a Vickers hardness tester (micro Vickers hardness tester, Zwick, Germany, ZHV μ) to measure the average hardness of three samples per case at a 100 g applied load and 15 s dwell time along the four radial directions. Figure 2 shows that each notch was the same distance from the centre of the disc to the edge.

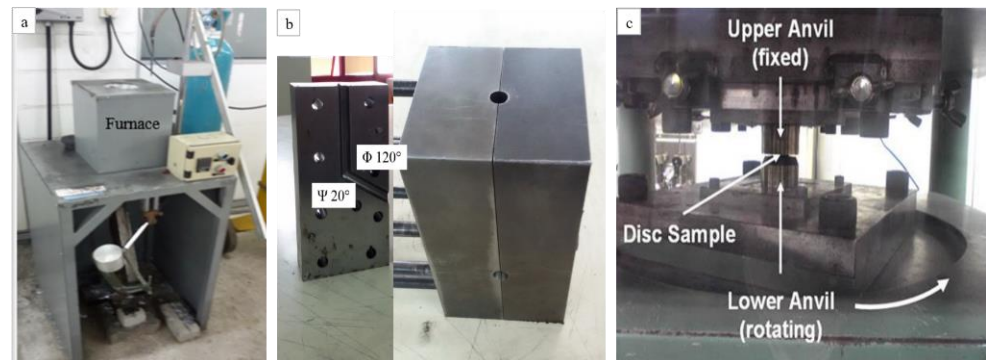


Figure 1. Schematic of (a) cooling slope casting, (b) ECAP die, and (c) HPT facility.

Microstructural micrograph areas at center and edge

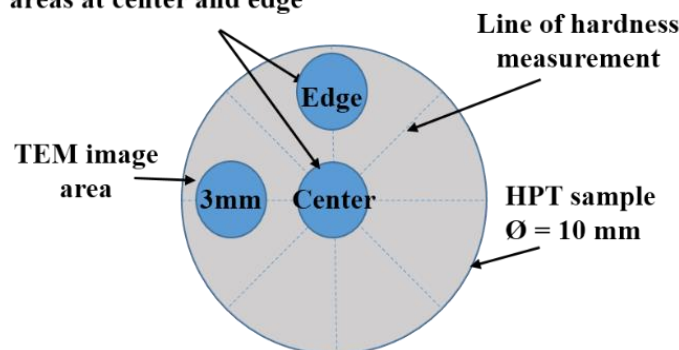


Figure 2. Schematic representation of the HPT disc and the location for measuring the disc hardness and the TEM area.

The as-cast, ECAPed, and HPTed sample preparation for microstructure analysis used silicon carbide (SiC) papers with grits between 180 and 2000 to polish the samples using $3\ \mu\text{m}$ and $1\ \mu\text{m}$ diamond paste (Al_2O_3). The etchant used in the etching process was Keller's reagent (1% HF, 1.5% HCl, 2.5% HNO_3 , H_2O solution). The microstructural characterisation of the samples was performed under a field-emission scanning electron microscope (FESEM, Zeiss, Oberkochen, Germany), field-emission scanning transmission electron microscope (FETEM, JEOL, JEM-2100F, Tokyo, Japan), and optical microscope (OM, Olympus Corporation, Tokyo, Japan). The microstructure was observed at the centre and close to the edge of the disc. The researchers conducted a quantitative metallography analysis to measure the grain size following ASTM E112 and used the Smart Tiffv2 software to measure the Si particle size (the length and width) using a minimum of 200 particles each time.

3. Results and Discussion

3.1. Microstructure of the As-Cast and Semisolid Al-Si Alloy Pre/Post T6

Optical micrographs of the as-cast sample in Figure 3a show the typical microstructure of an unmodified hypoeutectic Al-Si alloy, the primary α -Al phase, surrounded by coarse Si particles in the initial solidification phase in the eutectic (dark) phase. The dendritic grains are approximately 172 μm coarse eutectic Si particles. Figure 3b,c show the non-dendritic microstructure of the as-cast Al-Si alloy sample that resulted from shearing during the cooling slope and thixoforming process, where the primary α -Al phase was transformed into an almost spheroid shape with a size of 54 μm , while the Si particles transformed into fine needle-like particles. Figure 3d shows that the T6 heat treatment transformed the flake and needle-like morphology of the Si particles in the as-cast and thixoformed samples into angular and spherical shapes. During the solution heat treatment, the coarsening process fragmented and spheroidised the eutectic Si particles [11,29]. After the T6 heat treatment, the eutectic Si particles were refined, and their angular edges were not as sharp as in the as-cast alloy. Previous studies reported similar behaviour, where the T6 heat treatment process initiates the spheroidisation of Si particles [20,30].

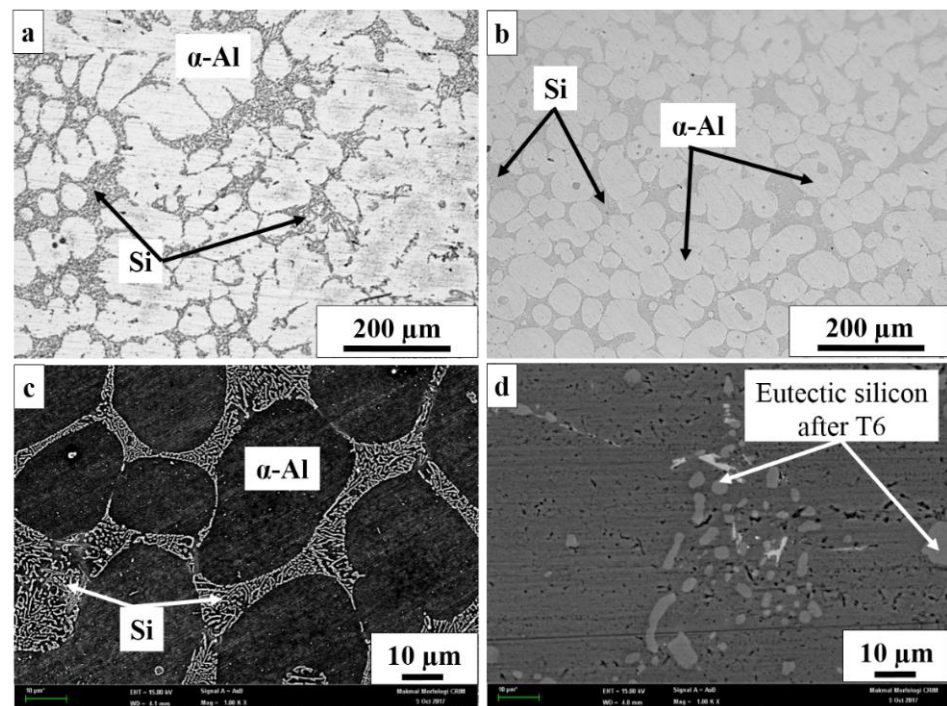


Figure 3. Optical micrographs of the pre-T6 (a) as-cast and (b) thixoformed samples. SEM micrograph of the thixoformed (c,d) post-T6 Si particles of thixoformed samples.

3.2. Microstructure of the ECAPed As-Cast and Thixoformed Samples after Two Passes Pre-/Post-T6

Figure 4a,b show the microstructure of the ECAPed as-cast sample and the heat-treated as-cast sample after two ECAP passes via route A, where the primary α -Al grain size of the Al-Si alloy is elongated, with some grains more elongated than others, and the grain boundaries are at approximately 45° . The microstructure is non-homogeneous, and the eutectic phase is erratically distributed in the matrix. The second ECAP pass significantly reduced the initial grain size in the as-cast and heat-treated as-cast samples from $\sim 172.31 \mu\text{m}$ to ~ 105.1 and $62.9 \mu\text{m}$, respectively. Figure 4a,b and Table 1 show that the Si particles and α -Al phase were refined after two ECAP passes, while the microstructure in the heat-treated sample was refined even further. The strain in the two ECAP passes elongated the α -Al phase. Figure 4c,d show the low and high magnification of the ECAPed

heat-treated thixoformed alloy samples after two passes, where the primary α -Al grains are enclosed by the Si eutectic phase in a heterogeneous microstructure. The α -Al grains remain agglomerated with a few longitudinal-shaped grains, which can be attributed to the material strength and the lack of elasticity of the thixoformed samples. There is some fragmentation of the Si particles among the elongated α -Al grains, as shown in Figure 4d. A higher number of ECAP passes caused crack formations on the surface of the thixoformed samples due to the high strength of the thixoformed alloy, as shown in Figure 4e.

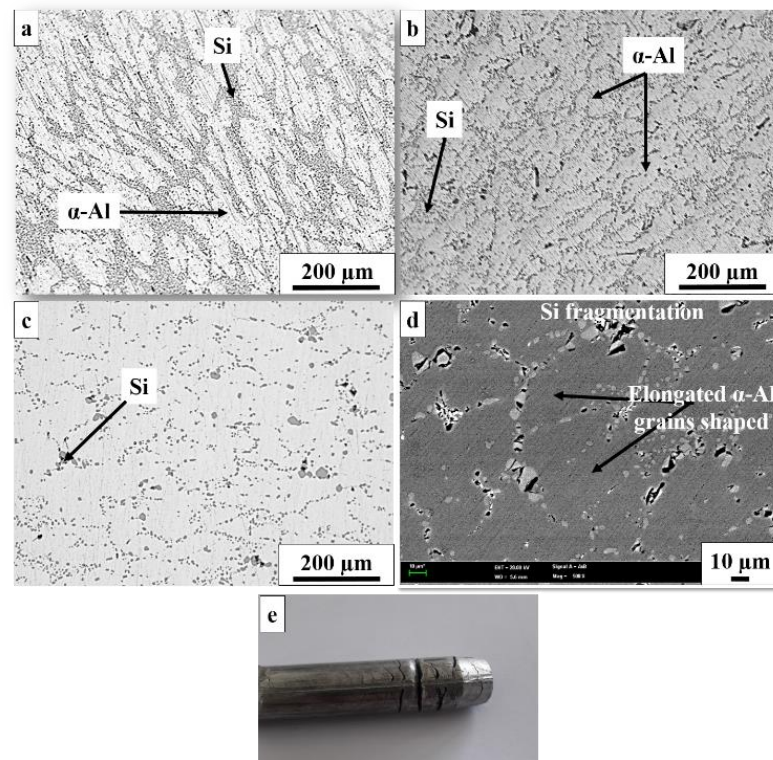


Figure 4. Optical micrograph of ECAPed Al-Si alloy samples after two passes. The (a) as-cast, (b) heat-treated as-cast, (c) heat-treated thixoformed, and (d) SEM enlargement of heat-treated thixoformed sample after two passes and (e) cracks on the thixoformed sample surface.

Table 1. Average grain size and Si particle size of ECAPed heat-treated as-cast and thixoformed Al-Si alloy.

Number of Passes	Si Particles Size (μm)	Grain Size (μm)
As-cast	4.22	172.31
As-cast, 2 passes	2.68	105.1
Heat treated as-cast, 2 passes	1.74	62.85
Thixoformed, 2 passes	3.10	72.12
Heat-treated thixoformed, 2 passes	1.21	47.50

3.3. Microstructure of the HPTed As-Cast and Thixoformed Al-Si Alloy Pre-/Post-T6 after 0.75 Turns

The researchers took an optical micrograph of the microstructure to evaluate the as-cast and thixoformed samples processed by HPT under a 6GPa pressure and 0.75 turns at two locations. Figure 2a,c show the optical micrograph at the disc centre, and Figure 2b,d are the optical micrograph for the location near the edge of the as-cast and thixoformed sample discs. Figure 5 is the optical micrograph of the centre and edge of the HPTed as-cast and thixoformed Al-Si alloy before T6. The centre of the as-cast sample shows

the presence of a large grain size in the primary α -Al phase, and the sample edge, which experienced the strain, shows the presence of a deformed dendrite shape. The morphology of the broken α -Al phase and eutectic phase is elongated in the shear flow direction, and the primary α -Al phase shows reduced thickness. The eutectic phase and Si particles are non-homogeneously distributed. Figure 5a,b show that, after 0.75 turns, the grains at the edge of the disc are finer than in the centre. The initial large coarse as-cast primary α -Al phase could be the reason for the big α -Al phase size in the as-cast sample. Figure 5c,d show there is no significant microstructural change in the centre of the thixoformed alloy relative to before applying HPT, while the edge of the alloy is elongated. The shape of the thixoformed alloy remained unchanged due to its high strength, and the low strain imposed on its centre reduces deformation. The eutectic Si particles at the edge of the alloy are non-homogeneous and less distributed.

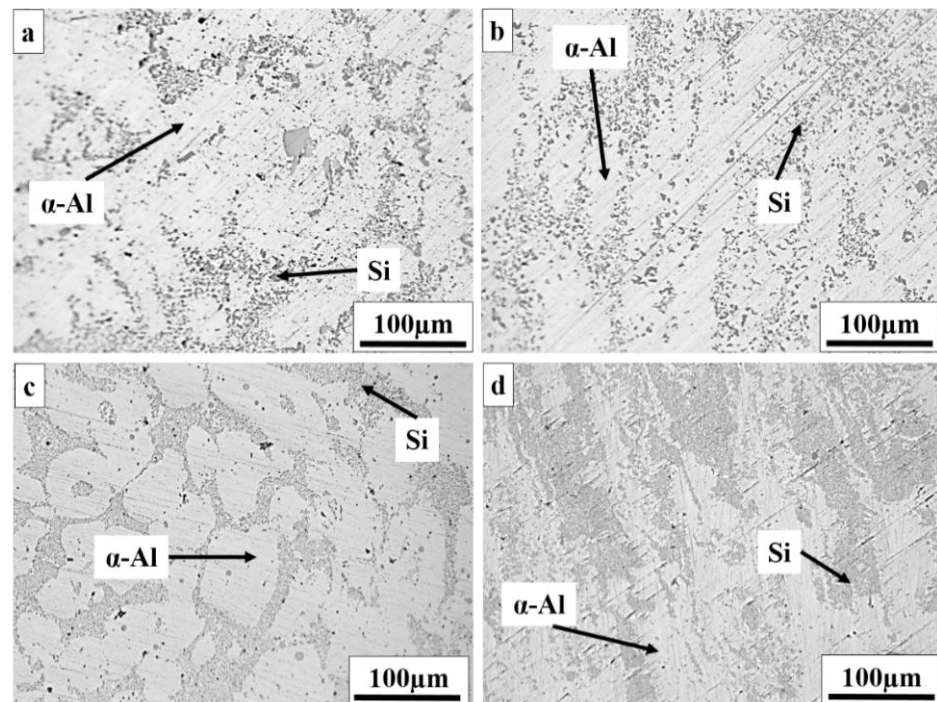


Figure 5. Optical micrographs at the centre and the edge of (a,b) as-cast and (c,d) thixoformed Al-Si alloy after 0.75 turns.

Figure 6a–d show the microstructure of the HPTed heat-treated as-cast and thixoformed Al-Si alloy after 0.75 turns.

The refined eutectic phase after heat treatment gives the microstructure of the Al-Si alloy higher workability, which has positive effects during HPT and further deforms and refines the microstructure. The α -Al phase is smaller, and the flake- and lamellar-shaped Si particles in the Al-Si alloy are finer. However, some large α -Al phase is still present, with a uniform spread of the Si particles and eutectic phase in the HPTed heat-treated samples compared to the Al-Si alloy samples processed by HPT without heat treatment. After 0.75 turns, the α -Al phase surrounded by the eutectic phase was still present in the centre of the pre-treated and post-heat-treated samples. The eutectic Si particles and eutectic phase are more homogeneously distributed at the edge than at the centre.

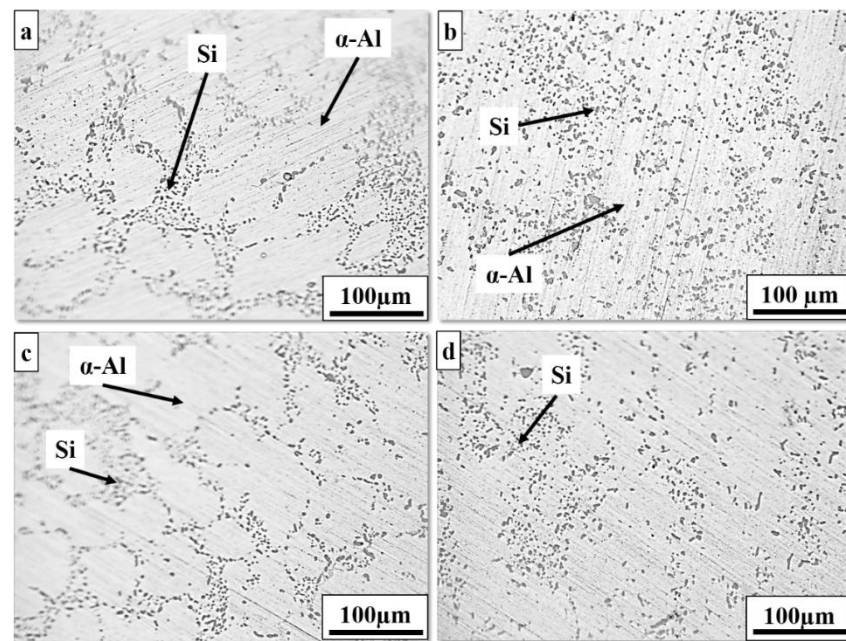


Figure 6. Optical micrograph of the centre and the edge of heat-treated (a,b) as-cast and (c,d) thixoformed Al-Si alloy after 0.75 turns.

3.4. Microstructure of the HPTed As-Cast and Thixoformed Pre-/Post-T6 after Five Turns

Figure 7 shows the mapping of the centre and the edge of the HPTed as-cast and thixoformed Al-Si alloy sample subjected to 6.0 GPa pressure after five turns. The mappings are for two locations, where (a,c) are the mapping of the disc centre, and (b,d) are the disc edge. During the HPT processing of the as-cast and thixoformed alloys, the primary α -Al phase was observed about 1 mm from the centre of the disc to the edge of the HPT disc, while the primary α -Al phase in the edge position completely disappeared. The higher number of turns increased the shear strain and resulted in a homogeneous and uniform Si particle distribution, as illustrated in Figure 7b,d. The eutectic Si particles at the edge of the as-cast sample are large relative to those in the thixoformed alloy. The eutectic Si particles are relatively homogeneously distributed in the aluminium matrixes in favour of fine Si particles in thixoformed, as observed at the edge, where the microstructure is homogeneous across the disc. The Si particles are broken into significantly smaller particles, thus considerably reducing the size of the Si particles. There is a much higher proportion of small Si particles and a much more homogeneously distributed microstructure, as demonstrated by [31].

Figure 8 shows the morphological map of the HPTed heat-treated as-cast and thixoformed Al-Si alloy at the centre and the edge of the sample after five turns.

The combination of heat-treated thixoforming and the HPT process resulted in a smaller Si particle size, and subsequent processing via HPT fragmented the Si particles because of the high imposed strain. The heat-treated thixoformed samples have more homogeneously distributed eutectic Si particles than the as-cast samples. The edge region has a finer microstructure than the central region in each processing revolution because of the higher torsional strain in the HPT process. The edges of the two alloys subjected to heat treatment have a very fine microstructure, and the alloying element is homogeneously distributed in the thixoformed sample than in the as-cast alloy after five turns. The higher torsional strain during HPT resulted in the edge region having a finer microstructure than the central region in each processing revolution. The following paragraph discusses in detail the distribution of eutectic Si particles and alloying elements at the edge of the as-cast and thixoformed alloys after T6. Figures 9 and 10 show the mapping of the intermetallic phase at the edge of the HPTed heat-treated as-cast and thixoformed Al-Si alloy sample after being subjected to a 6.0 GPa pressure for five turns. A comparison of the

two figures showed that the distribution, homogeneity, and refinement of the eutectic Si particles and the alloying elements at the edge of the heat-treated thixoformed alloy are more appropriate than as-cast alloy, indicating that applying heat treatment before HPT processing significantly influences the final size and distribution of large silicon particles after straining. The breakdown of intermetallic phases of the Al-Si alloy is due to the high strains imposed on the Al-Si alloy during HPT processing through higher rotational revolutions, which reduces the Si particle size and the homogeneous dispersion of the fragmented particles.

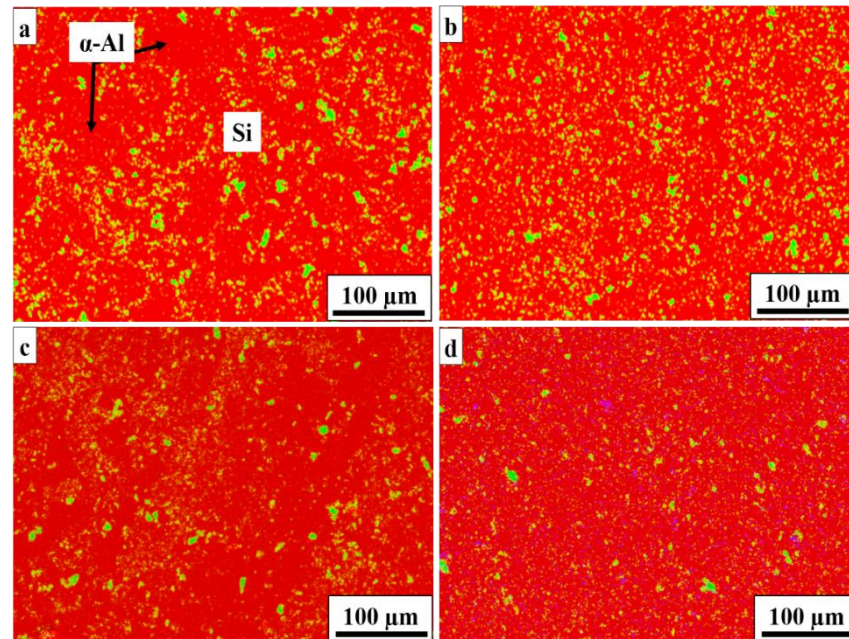


Figure 7. Morphological map of the Si particles (green) in the Al matrix (red) before heat treatment at the centre and the edge of the as-cast (a,b) and thixoformed (c,d) after five turns.

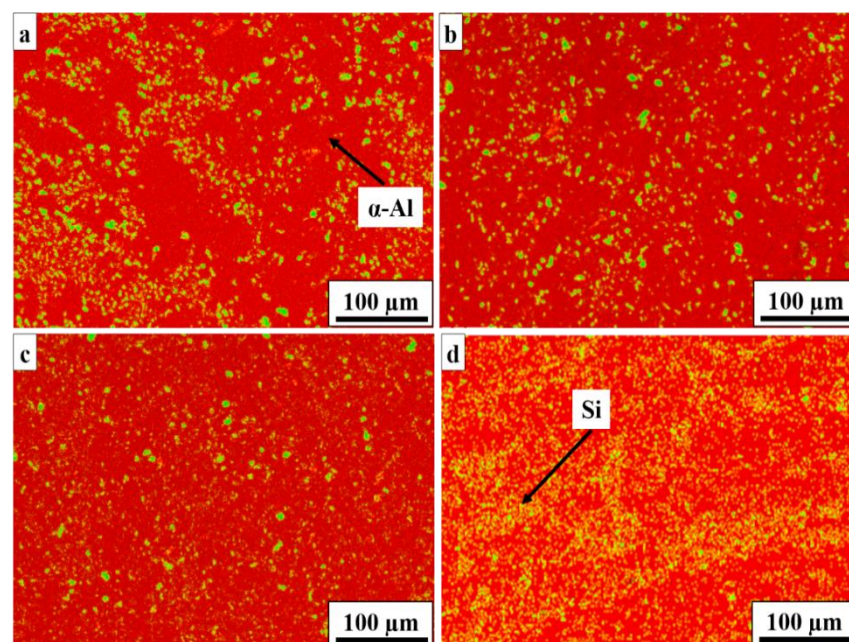


Figure 8. Morphological map of the Si particles (green) in the Al matrix (red) after heat treatment at the centre and the edge of the as-cast (a,b) and thixoformed (c,d) after five turns.

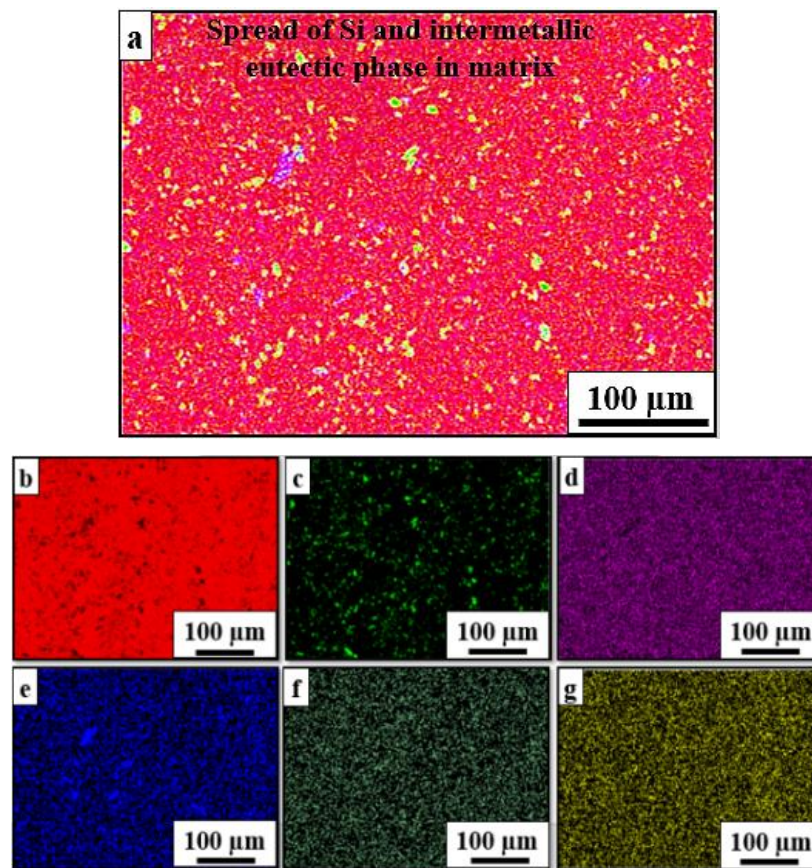


Figure 9. Mapping of HPTed heat-treated (a) as-cast (b) Al, (c) Si, (d) Mg, (e) Fe, (f) Ti, and (g) Cu in the edge position of Al-Si alloy after five turns.

Figure 11 shows FETEM micrographs of the heat-treated thixoformed Al-Si alloy samples processed by HPT after five turns. The FETEM micrograph shows the presence of many dislocations and subgrains.

The dislocations are present in many grains, particularly those close to the grain boundaries. The large grains indicate that gallium (Ga) irradiation during ion milling causes significant static recrystallisation. It is worth noting that ion milling using 30 keV (Ga) ions for 180 min resulted in considerable dynamic recovery and smooth grain boundaries. These observations suggest that ultrafine-grained materials must be handled carefully before evaluation [32]. A high number of HPT processing cycles produces high shear strains because of the high dislocation density attributable to grain refinement and higher microhardness [33–35]. The microstructure, comprising subgrains and a dislocation cell structure, is due to the severe plastic deformation during the HPT process. However, the FETEM micrograph of the HPTed heat-treated thixoformed Al-Si alloy showed a high dislocation density and ultrafine-grained structure. The dislocations can move and interact with each other during the shear strain process, forming a dislocation cell structure having a high dislocation density. The imposition of further strain resulted in the formation of subgrain boundaries due to the dislocation agglomeration. The coarse grains are fragmented into a lamellae microstructure, as shown in Figure 10b. Cu produced by HPT processing shows a similar trend [36].

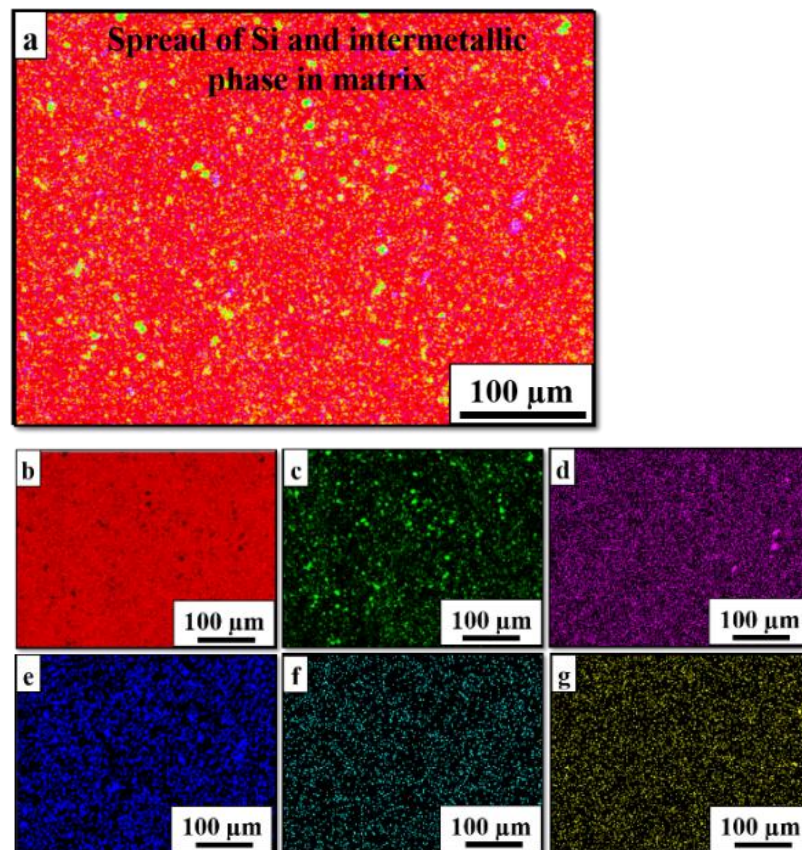


Figure 10. Mapping of HPTed heat-treated (a) and thixoformed (b) Al, (c) Si, (d) Mg, (e) Fe, (f) Ti, and (g) Cu in the edge position of Al-Si alloy respectively after five turns.

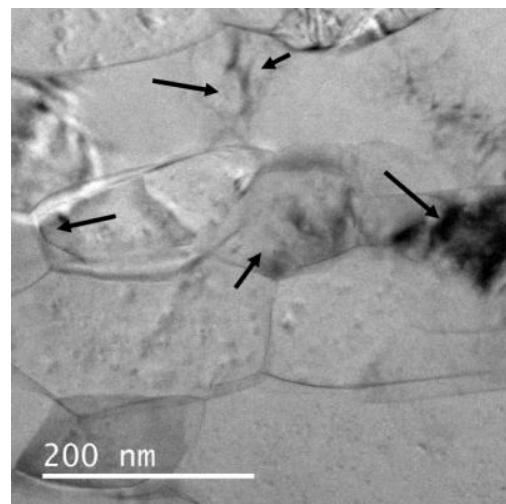


Figure 11. TEM image of subgrains in HPTed heat-treated thixoformed sample after five turns.

Figure 11 shows the formation of many dislocations and subgrains. The micrographs show a markedly smaller grain size of the undeformed material. Previous research has described similar dislocation clustering in semisolid cast alloys when using the cooling slope method [37]. However, using severe plastic deformation in the subsequent processing of the thixoformed alloys produced a higher dislocation density and finer subgrains. Figure 12 shows that the edge of the heat-treated thixoformed Al-Si alloy processed by HPT after five turns has very fine grains separated by low misorientation angles and well-defined grains with an average size of ~130 nm within the aluminium matrix. Further strain on the sample

caused the aggregation of dislocations and the formation of subgrain boundaries. Increasing the number of turns in the HPT process causes higher deformation, which increases their misorientation gradually until the final transformation into high-angle boundaries under high strain [38,39]. As anticipated, most dislocations are due to the normal deformation mode, resulting in the dislocations coalescing to form subgrains. The grain refinement of this alloy can be achieved in a manner similar to earlier observations [36,40]. Significant strain hardening occurs due to the higher accumulated strain energy through the increased dislocations. As the strain increases, the subgrains become finer, while the dislocation density in the subgrains increases. The subgrain boundaries become better defined by increased misorientation angles between adjacent grains.

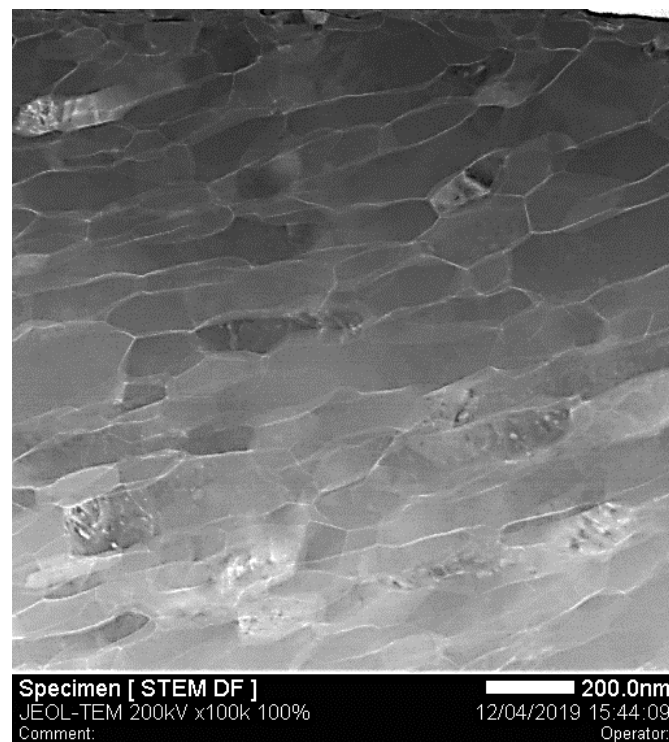


Figure 12. TEM image of a heat-treated thixoformed sample after five turns of HPT.

3.5. Hardness of ECAPed and HPTed As-Cast and Thixoformed Pre-/Post-T6

Figure 13a presents the Vickers microhardness of the as-cast and thixoformed samples; the measurements were made after subjecting the Al-Si alloy samples to a combination of heat treatment and ECAP via route A. The Al-Si alloys showed higher hardness after the thixoforming process because the microstructure was transformed into a globular structure. The heat treatment by thixoforming increases the hardness of the Al-Si alloys from 61 HV to 99.85 Hv. The shear force breaks the dendrite arms of the primary α -Al phase and refines the grains. The Al-Si alloys show a smaller and denser microstructure after the cooling slope condition, having a higher microhardness than the as-cast Al-Si alloy sample [41]. The transformation of the morphology of Si particles in the as-cast Al-Si alloy sample from flake-shaped into lamellar and acicular shapes during the thixoforming process increases its microhardness. The thixoforming process applies a high pressure that increases the cooling rate, refines the α -Al grains, and transforms the Si morphology into a fine circular grain. The casting process in thixoforming eliminates porosity and causes shrinkage, thus increasing the alloy's hardness. The shape and distribution of the eutectic Si particles are much more uniform than in the as-cast samples. Spheroidised eutectic Si after the T6 heat treatment increases the sample hardness. Generally, the spheroidised Si particles subsequent to the T6 heat treatment and the precipitation of magnesium silicide (Mg_2Si) particles in the ageing process enhance the Al-Si alloy's ultimate tensile strength and

hardness [8,42]. This increases the dislocation density, grain refinement, and fragmentation of eutectic Si particles during the ECAP process, thereby significantly increasing hardness; this result is consistent with the findings of previous studies [43–45].

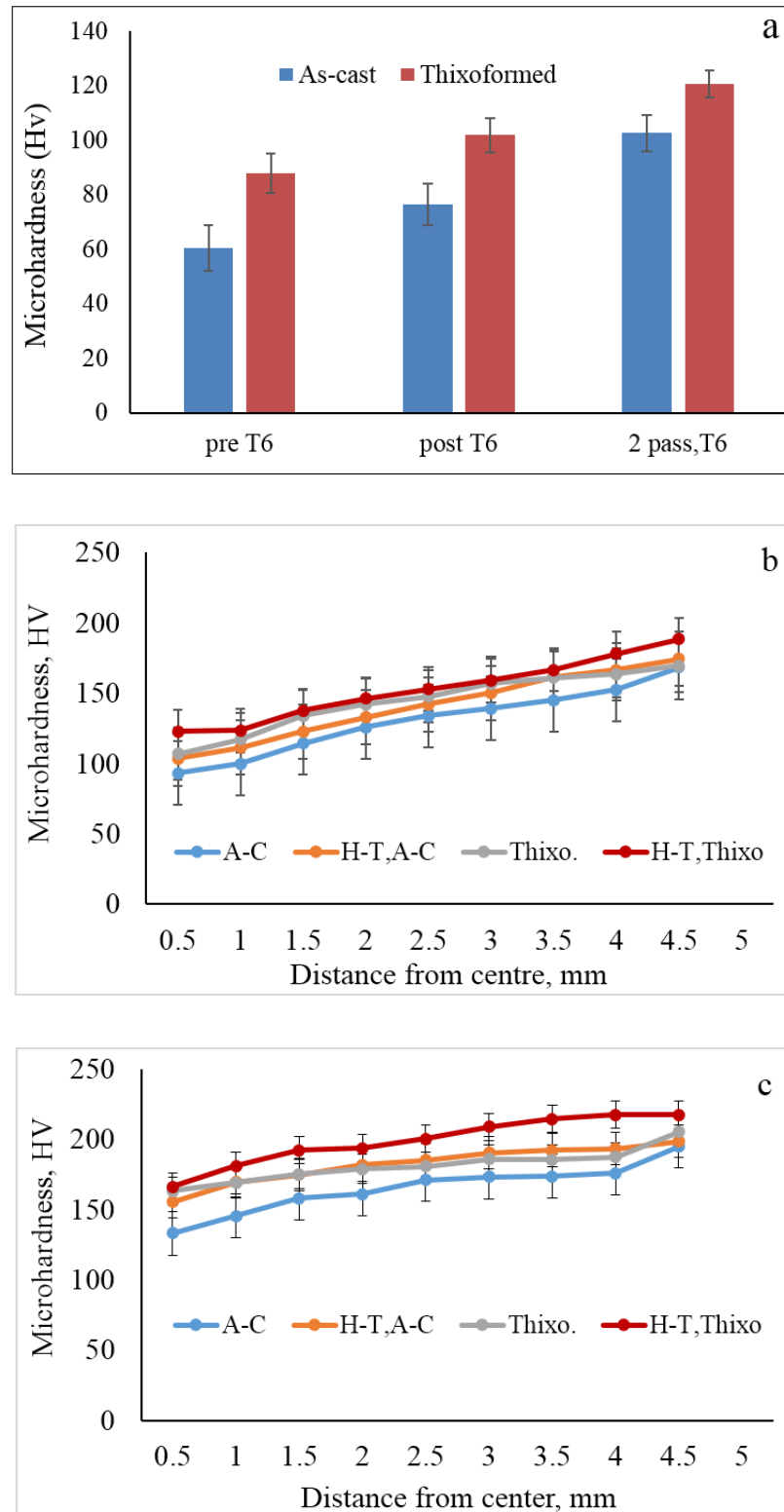


Figure 13. Microhardness of the Al-Si alloy (a) after ECAP, (b) 0.75 turns and (c) 5 turns of HPT process.

Figure 13b,c show the average Vickers microhardness across the diameter of each as-cast and thixoformed disc before and after T6 heat treatment and 0.75 and 5 turns of HPT under a 6.0 GPa pressure. The researchers examined the change in hardness along the disc diameter at a constant distance of 0.5 mm from the axes of each processed disc. The disc hardness increases significantly after 0.75 turns, where the increase in hardness in the disc periphery is higher than at the centre of the discs. The HPT process considerably increases the hardness of the as-cast Al-Si alloy from the initial 60.7 Hv microhardness. The hardness between the centre and the edge of the disc varies depending on the number of turns. The increase in hardness is more marked after 5 turns than after 0.75 turns. Figure 13 shows the increase in hardness along the disc axis from the centre to the perimeter. After five turns, the edge of the disc shows a homogeneous distribution of eutectic Si particles and intermetallic compounds and grain refinement, which contribute to the increased hardness. This result is similar to the microstructures shown in Figures 6–9, where the eutectic Si particles and intermetallic compounds in the treated sample are smaller and more evenly distributed after 5 turns than after 0.75 turns of HPT. A higher number of turns in the HPT process leads to a high shear strain associated with the high dislocation density related to grain refinement and increased microhardness [31,33,34,46,47]. Most discs showed a typical hardness gradient due to strain hardening behaviour [48], where hardness was lower in the centre of the disc and gradually increased towards the edge of the disc with a corresponding strain increase in the HPT process.

The application of ECAP or HPT after heat treatment to semisolid materials resulted in a more refined microstructure and the redistribution of Si and the intermetallic phase. The increasing hardness is associated with the fragmentation and redistribution of eutectic Si and intermetallic compounds because the high strain during the ECAP and HPT processes increases the dislocation density and grain refinement. The thixoformed sample has a higher microhardness than the as-cast sample as the semisolid microstructure becomes smaller and denser [41], and the morphology of Si particles in the as-cast sample changes from flake-like into a fine needle-like shape, as in the thixoformed sample. Increasing the number of revolutions in HPT processing produces high shear strains associated with the high dislocation density associated with grain refinement and higher microhardness [33–35]. These results are consistent with the earlier report on an aluminium alloy with a higher hardness after processing with a combination of heat treatment and semi-hard treatment followed by ECAP processing. The results are congruent with previous findings that aluminium alloys have a higher hardness after being subjected to heat treatment and semisolid processing, followed by ECAP [21,22].

4. Conclusions

This study investigated the impact of microstructural refinement on the hardness of the Al-Si alloy processed by a combination of T6 heat treatment and HPT. Based on the investigation results, the researchers have made the following conclusions.

1. Refining the microstructure of the Al-Si alloy through a combination of thixoforming and heat treatment before SPD produces a more homogeneous and finer microstructure than without heat treatment.
2. The thixoformed samples after T6 heat treatment followed by ECAP reach up to two passes. Increasing the number of ECAP passes resulted in crack formation on the surface of the thixoformed samples due to the high strength of the thixoformed alloy.
3. Combining thixoforming and heat treatment followed by five revolutions of HPT processing at a pressure of 6.0 GPa and room temperature produces a hypoeutectic Al-Si alloy with an ultrafine microstructure and a homogeneous distribution of the eutectic Si particles and intermetallic compounds.
4. Increasing the number of ECAP passes and the number of turns in HPT after the combination of thixoforming and heat treatment resulted in the significantly higher hardness of the hypoeutectic Al-Si alloy.

Author Contributions: M.A.G. carried out the experimental works, analysis, and writing under the supervision of M.Z.O., N.K.O., I.F.M. and O.M.I. All authors have read and agreed to the published version of the manuscript.

Funding: This research received no external funding.

Institutional Review Board Statement: Not applicable.

Informed Consent Statement: Not applicable.

Data Availability Statement: Not applicable.

Acknowledgments: The researchers would like to thank the Deanship of Scientific Research, Qassim University, for funding the publication of this project.

Conflicts of Interest: The authors declare no conflict of interest.

References

1. Haghdadadi, N.; Zarei-Hanzaki, A.; Abedi, H.R.; Sabokpa, O. The effect of thermomechanical parameters on the eutectic silicon characteristics in a non-modified cast A356 aluminum alloy. *Mater. Sci. Eng. A* **2012**, *549*, 93–99. [[CrossRef](#)]
2. Davis, J.R. Aluminum and Aluminum Alloys. *Light Met. Alloys* **2001**, *66*, 351–416. [[CrossRef](#)]
3. Galvin, E.; O'Brien, D.; Cummins, C.; Mac Donald, B.J.; Lally, C. A strain-mediated corrosion model for bioabsorbable metallic stents. *Acta Biomater.* **2017**, *55*, 505–517. [[CrossRef](#)]
4. Birol, Y. A357 thixoforming feedstock produced by cooling slope casting. *J. Mater. Process. Technol.* **2007**, *186*, 94–101. [[CrossRef](#)]
5. Haga, T.; Kapranos, P. Billetless simple thixoforming process. *J. Mater. Process. Technol.* **2002**, *130–131*, 581–586. [[CrossRef](#)]
6. Das, P.; Samanta, S.K.; Venkatpathi, B.R.K.; Chattopadhyay, H.; Dutta, P. Microstructural evolution of A356 Al alloy during flow along a cooling slope. *Trans. Indian Inst. Met.* **2012**, *65*, 669–672. [[CrossRef](#)]
7. Salleh, M.S.; Omar, M.Z.; Alhawari, K.S.; Mohammed, M.N.; Ali, M.A.M.; Mohamad, E. Microstructural evolution and mechanical properties of thixoformed A319 alloys containing variable amounts of magnesium. *Trans. Nonferrous Met. Soc. China (Engl. Ed.)* **2016**, *26*, 2029–2042. [[CrossRef](#)]
8. Möller, H.; Govender, G.; Stumpf, W. Factors Influencing Tensile Mechanical Properties Of Al-7Si-Mg Casting Alloys A356/7. In *Light Metals*; Springer: New York, NY, USA, 2012; pp. 467–471.
9. Nguyen, V.T.; Hussain, Z.; Anasyida, A.S.; Huy, T.D.; Almanar, I.P. Influence of Semi-Solid Casting and Equal Channel Pressing on Microstructure of a Hypoeutectic Al-Si Alloy. *Mater. Sci. Forum* **2015**, *819*, 9–14. [[CrossRef](#)]
10. Mohamed, A.M.A.; Samuel, F.H. A Review on the Heat Treatment of Al-Si-Cu/Mg Casting Alloys. *Conv. Nov. Appl.* **2012**, *229*, 422. [[CrossRef](#)]
11. Ogris, E.; Wahlen, A.; Lüchinger, H.; Uggowitzer, P.J. On the silicon spheroidization in Al-Si alloys. *J. Light Met.* **2002**, *2*, 263–269. [[CrossRef](#)]
12. Moradi, M.; Nili-Ahmadabadi, M.; Heidarian, B. Improvement of mechanical properties of AL (A356) cast alloy processed by ecap with different heat treatments. *Int. J. Mater. Form.* **2009**, *2*, 85–88. [[CrossRef](#)]
13. Bastidas, J.M.; Forn, A.; Torres, C.L.; Baile, M.T.; Polo, J.L. Pitting corrosion of A357 aluminium alloy obtained by semisolid processing. *Mater. Corros.* **2001**, *52*, 691–696. [[CrossRef](#)]
14. Mingo, B.; Arrabal, R.; Pardo, A.; Matykina, E.; Skeldon, P. 3D study of intermetallics and their effect on the corrosion morphology of rheocast aluminium alloy. *Mater. Charact.* **2016**, *112*, 122–128. [[CrossRef](#)]
15. Wang, Q.G.; Praud, M.; Needleman, A.; Kim, K.S.; Griffiths, J.R.; Davidson, C.J.; Cáceres, C.H.; Benzerger, A.A. Size effects in aluminium alloy castings. *Acta Mater.* **2010**, *58*, 3006–3013. [[CrossRef](#)]
16. Garcia-Infanta, J.M.; Zhilyaev, A.P.; Cepeda-Jiménez, C.M.; Ruano, O.A.; Carreño, F. Effect of the deformation path on the ductility of a hypoeutectic Al-Si casting alloy subjected to equal-channel angular pressing by routes A, BA, BC and C. *Scr. Mater.* **2008**, *58*, 138–141. [[CrossRef](#)]
17. Langdon, T.G. The principles of grain refinement in equal-channel angular pressing. *Mater. Sci. Eng. A* **2007**, *462*, 3–11. [[CrossRef](#)]
18. Saito, Y. Ultra-fine grained bulk aluminum produced by accumulative roll-bonding (ARB) process. *Scr. Mater.* **1998**, *39*, 1221–1227. [[CrossRef](#)]
19. Łyszkowski, R. Influence of Strain Route Changes on the Microstructure and Mechanical Properties of CuZn36 Alloy during Cross Channel Extrusion CCE. *Materials* **2022**, *15*, 1124. [[CrossRef](#)] [[PubMed](#)]
20. Ishak, N.N.M.; Salleh, M.S.; Yahaya, S.H.; Mohamad, E.; Sulaiman, M.A. The Effect of Equal Channel Angular Pressing (ECAP) on the Microstructure and Hardness of A356 Aluminium Alloy. *J. Adv. Manuf. Technol.* **2017**, *11*, 47–58.
21. Natori, K.; Utsunomiya, H.; Tanaka, T. Improvement in formability of semi-solid cast hypoeutectic Al-Si alloys by equal-channel angular pressing. *J. Mater. Process. Technol.* **2017**, *240*, 240–248. [[CrossRef](#)]
22. Van Thuong, N.; Zuhailawati, H.; Seman, A.A.; Huy, T.D.; Dhindaw, B.K. Microstructural evolution and wear characteristics of equal channel angular pressing processed semi-solid-cast hypoeutectic aluminum alloys. *Mater. Des.* **2015**, *67*, 448–456. [[CrossRef](#)]
23. Nomura, F.; Matsuba, T.; Tanaka, T.; Imaida, Y. Improvement of mechanical properties of semi-solid alloys by ECAP processing. In *Advanced Materials Research*; Trance Tech Publication: Stafa-Zurich, Switzerland, 2010; Volume 123–125, pp. 483–486. [[CrossRef](#)]

24. Gebril, M.A.; Omar, M.Z.; Mohamed, I.F.; Othman, N.K. Microstructural Evaluation and Corrosion Resistance of Semisolid Cast A356 Alloy Processed by Equal Channel Angular Pressing. *Metals* **2019**, *9*, 303. [[CrossRef](#)]
25. Nejadseyfi, O.; Shokuhfar, A.; Dabiri, A.; Azimi, A. Combining equal-channel angular pressing and heat treatment to obtain enhanced corrosion resistance in 6061 aluminum alloy. *J. Alloys Compd.* **2015**, *648*, 912–918. [[CrossRef](#)]
26. Gebril, M.A.; Omar, M.Z.; Mohamed, I.F.; Othman, N.K.; Irfan, O.M. Combining Heat Treatment and High-Pressure Torsion to Enhance the Hardness and Corrosion Resistance of A356 Alloy. *Metals* **2022**, *12*, 853. [[CrossRef](#)]
27. Samsudin, M.; Omar, M.Z.; Abdullah, S. Effects of rheocasting and thixoforming on the microstructure and mechanical properties of A356 aluminium alloy. *J. Teknol.* **2016**, *78*, 107–113. [[CrossRef](#)]
28. Rooy, E.L.; Linden, J.H.L. *Van ASM Metals Handbook, Vol 02 Properties and Selection: Nonferrous Alloys and Special-Purpose Materials*; ASM International: Geauga, OH, USA, 1990; pp. 3330–3345. [[CrossRef](#)]
29. Tiryakioğlu, M. Si particle size and aspect ratio distributions in an Al-7%Si-0.6%Mg alloy during solution treatment. *Mater. Sci. Eng. A* **2008**, *473*, 1–6. [[CrossRef](#)]
30. Li, B.; Wang, H.; Jie, J.; Wei, Z. Effects of yttrium and heat treatment on the microstructure and tensile properties of Al-7.5Si-0.5Mg alloy. *Mater. Des.* **2011**, *32*, 1617–1622. [[CrossRef](#)]
31. Cepeda-Jiménez, C.M.; García-Infanta, J.M.; Ruano, O.A.; Carreño, F. Mechanical properties at room temperature of an Al-Zn-Mg-Cu alloy processed by equal channel angular pressing. *J. Alloys Compd.* **2011**, *509*, 8649–8656. [[CrossRef](#)]
32. Edalati, K.; Horita, Z.; Furuta, T.; Kuramoto, S. Dynamic recrystallization and recovery during high-pressure torsion: Experimental evidence by torque measurement using ring specimens. *Mater. Sci. Eng. A* **2013**, *559*, 506–509. [[CrossRef](#)]
33. Nie, M.; Wang, C.T.; Qu, M.; Gao, N.; Wharton, J.A.; Langdon, T.G. The corrosion behaviour of commercial purity titanium processed by high-pressure torsion. *J. Mater. Sci.* **2014**, *49*, 2824–2831. [[CrossRef](#)]
34. El Aal, M.I.A.; Kim, H.S. Wear properties of high pressure torsion processed ultrafine grained Al-7% Si alloy. *Mater. Des.* **2014**, *53*, 373–382. [[CrossRef](#)]
35. Wang, X.; Nie, M.; Wang, C.T.; Wang, S.C.; Gao, N. Microhardness and corrosion properties of hypoeutectic Al-7Si alloy processed by high-pressure torsion. *Mater. Des.* **2015**, *83*, 193–202. [[CrossRef](#)]
36. Edalati, K.; Fujioka, T.; Horita, Z. Microstructure and mechanical properties of pure Cu processed by high-pressure torsion. *Mater. Sci. Eng. A* **2008**, *497*, 168–173. [[CrossRef](#)]
37. Barekar, N.S.; Pradhan, R.; Dhindaw, B.K. Mechanism of microstructural refinement of al-cu alloy during low melt sheared slope casting. *J. Mater. Eng. Perform.* **2014**, *23*, 439–443. [[CrossRef](#)]
38. Descartes, S.; Desrayaud, C.; Rauch, E.F. Inhomogeneous microstructural evolution of pure iron during high-pressure torsion. *Mater. Sci. Eng. A* **2011**, *528*, 3666–3675. [[CrossRef](#)]
39. Cepeda-Jiménez, C.M.; Orozco-Caballero, A.; García-Infanta, J.M.; Zhilyaev, A.P.; Ruano, O.A.; Carreño, F. Assessment of homogeneity of the shear-strain pattern in Al-7 wt.% Si casting alloy processed by high-pressure torsion. *Mater. Sci. Eng. A* **2014**, *597*, 102–110. [[CrossRef](#)]
40. Ito, Y.; Horita, Z. Microstructural evolution in pure aluminum processed by high-pressure torsion. *Mater. Sci. Eng. A* **2009**, *503*, 32–36. [[CrossRef](#)]
41. BoChao, L.; YoungKoo, P.; HongSheng, D. Effects of rheocasting and heat treatment on microstructure and mechanical properties of A356 alloy. *Mater. Sci. Eng. A* **2011**, *528*, 986–995. [[CrossRef](#)]
42. Zhu, M. Effects of T6 heat treatment on the microstructure, tensile properties, and fracture behavior of the modified A356 alloys. *J. Mater.* **2017**, *36*, 243–249. [[CrossRef](#)]
43. Cepeda-Jiménez, C.M.; García-Infanta, J.M.; Zhilyaev, A.P.; Ruano, O.A.; Carreño, F. Influence of the supersaturated silicon solid solution concentration on the effectiveness of severe plastic deformation processing in Al-7 wt.% Si casting alloy. *Mater. Sci. Eng. A* **2011**, *528*, 7938–7947. [[CrossRef](#)]
44. Goodarzy, M.H.; Arabi, H.; Boutorabi, M.A.; Seyedein, S.H.; Najafabadi, S.H.H. The effects of room temperature ECAP and subsequent aging on mechanical properties of 2024 Al alloy. *J. Alloys Compd.* **2014**, *585*, 753–759. [[CrossRef](#)]
45. Kumar, S.R.; Gudimetla, K.; Venkatachalam, P.; Ravisankar, B.; Jayasankar, K. Microstructural and mechanical properties of Al 7075 alloy processed by Equal Channel Angular Pressing. *Mater. Sci. Eng. A* **2012**, *533*, 50–54. [[CrossRef](#)]
46. Loucif, A.; Figueiredo, R.B.; Baudin, T.; Brisset, F.; Langdon, T.G. Microstructural evolution in an Al-6061 alloy processed by high-pressure torsion. *Mater. Sci. Eng. A* **2010**, *527*, 4864–4869. [[CrossRef](#)]
47. Ghosh, K.S.; Gao, N.; Starink, M.J. Characterisation of high pressure torsion processed 7150 Al-Zn-Mg-Cu alloy. *Mater. Sci. Eng. A* **2012**, *552*, 164–171. [[CrossRef](#)]
48. Kawasaki, M. Different models of hardness evolution in ultrafine-grained materials processed by high-pressure torsion. *J. Mater. Sci.* **2014**, *49*, 18–34. [[CrossRef](#)]